



tissues, cells or experimental conditions, and have been applied in a variety of genomic contexts. For example, Luo and Zhao [7] jointly modeled protein-protein interactions across different experimental levels of single-cell interventions within a Bayesian framework. In the context of QTL mapping, instead of conducting association tests for each genetic variant and trait separately (*univariate association screening*), Bayesian models are applied to jointly detect QTL effects for multiple traits [8] or to combine data from different tissues and cell types [9, 10]. One fundamental aspect of hierarchical models, such as *hierarchically linked regressions*, is the use of “local” parameters specific to each unit (or regression) and “global” parameters shared across units, which are involved in the prior specification of the local parameters. Global parameters help to learn the overall characteristics of the problem such as sparsity levels, typical effect sizes and noise levels, while local parameters define the specific characteristics of the unit in question. Such a structure can largely increase statistical power in particular when some weak effects are shared.

However, Bayesian hierarchical inference for genomics data usually involves obtaining complex, high-dimensional posterior distributions, which requires large computational resources. It is therefore rarely applied to biobank-scale data analysis, despite its relevance for uncovering biologically meaningful patterns with enhanced statistical power. Recent developments in scalable Bayesian inference have brought deterministic approximations to the forefront, providing a more efficient solution than traditional sampling-based methods like Markov Chain Monte Carlo (MCMC). In particular, variational inference (VI) algorithms approximate the posterior using simpler families of distributions, such as fully-factorized distributions in the case of mean-field VI [see, e.g., 11]. Under global-local Bayesian model hierarchies, mean-field VI usually approximates the posterior into a product where the “factors” are split between local or global parameters. When the dimensionality is high (i.e., when the number of units is large, which is typical in genomics), a large number of local parameters need updating in turn, while holding the others fixed. When the sample size is large, each update is also computationally expensive. Therefore, although VI-based Bayesian hierarchical models have been proposed for relatively large problems, such approaches are still not nimble for processing genome-wide data in today’s biobanks.

Current VI implementations of hierarchical models also often overlook an important feature defining most omics problems: while the total number of modeled units may be large, meaningful biological signals are typically concentrated in only a small subset of “active” local units. Exploiting this sparsity, adaptively focusing update efforts on these active units (in a way we are going to make precise in this work) could improve the algorithm’s scalability without sacrificing accuracy. Following this observation, we propose an “adaptive focus” strategy for CAVI, designed to enhance the scalability of Bayesian hierarchical models for sparse, high-dimensional problems. At each iteration, the algorithm evaluates the activity of each unit based on a criterion (using the current posterior estimates), and accordingly defines an “activity score” for each unit. This score is dynamically adjusted throughout the algorithm, leading to an *adaptive selection process* that updates only a subset of parameters corresponding to active units. In this paper, we formulate the concept of AF-CAVI under a general global-local framework, and provide an example of AF-CAVI implementation for protein quantitative trait locus (pQTL) mapping and particularly for the detection of hotspots (loci associated with many traits) in a biobank-scale dataset.

The rest of the paper is organized as follows: Section 2 and Section 3 provide an overview of CAVI under the “global-local” framework and the adaptive focus strategy. Section 4 evaluates the computational efficiency and performance of AF-CAVI using simulated and real datasets. Finally, Section 5 summarizes the key results and discusses their implications for future research.

## 2 CAVI under the “global-local” decomposition

Given  $n$  independent and identically distributed samples, let  $\mathbf{X} = (X_1, \dots, X_p)$  represent an  $n \times p$  matrix of candidate predictors and  $\mathbf{y} = (\mathbf{y}_1, \dots, \mathbf{y}_q)$ , an  $n \times q$  response matrix composed of  $q$  units. Further assume a model where the relationship between  $\mathbf{X}$  and unit  $\mathbf{y}_t$ ,  $t = 1, \dots, q$ , is governed by a local parameter vector  $\boldsymbol{\nu}_t^l$ , and where information is shared across local units through a global parameter vector  $\boldsymbol{\nu}^g$  which defines the prior distribution over the local parameters  $\boldsymbol{\nu}_t^l$ . Denote  $\boldsymbol{\nu}^l = (\boldsymbol{\nu}_1^l, \dots, \boldsymbol{\nu}_q^l)$ , the vector of local parameters, and  $\boldsymbol{\nu} = (\boldsymbol{\nu}^l, \boldsymbol{\nu}^g)$ , the vector of all parameters. Then, the joint log-probability of the global-local hierarchical model decomposes as:

$$\log p(\mathbf{y}, \boldsymbol{\nu}) = \log p(\boldsymbol{\nu}^g) + \sum_t \log p(\mathbf{y}, \boldsymbol{\nu}_t^l | \boldsymbol{\nu}^g).$$

Reflecting the conditional independence structure across local units given the global parameter vector  $\boldsymbol{\nu}^g$ , the posterior distribution can be decomposed as:

$$\log p(\boldsymbol{\nu} | \mathbf{y}) = \log p(\boldsymbol{\nu}^g | \mathbf{y}) + \sum_t \log p(\boldsymbol{\nu}_t^l | \boldsymbol{\nu}^g, \mathbf{y}). \quad (1)$$

Variational inference aims to approximate the posterior  $p(\boldsymbol{\nu} | \mathbf{y})$  with a “variational” distribution  $q(\boldsymbol{\nu})$  by minimizing the reverse Kullback-Leibler divergence (KL divergence):

$$\begin{aligned} \text{KL} [q(\boldsymbol{\nu}) || p(\boldsymbol{\nu} | \mathbf{y})] &= \mathbb{E}_q[\log q(\boldsymbol{\nu})] - \mathbb{E}_q[\log p(\boldsymbol{\nu} | \mathbf{y})] \\ &= -\mathbb{E}_q \left[ \log \frac{p(\boldsymbol{\nu}, \mathbf{y})}{q(\boldsymbol{\nu})} \right] + \log p(\mathbf{y}). \end{aligned}$$

It can therefore be seen that, to avoid computing the log evidence  $\log p(\mathbf{y})$ , the minimization of KL divergence can be transformed into a maximization problem, i.e., optimizing the so-called Evidence Lower Bound (ELBO):

$$\begin{aligned} \mathcal{L}(q) &= \mathbb{E}_q \left[ \log \frac{p(\boldsymbol{\nu}, \mathbf{y})}{q(\boldsymbol{\nu})} \right] \\ &= \mathbb{E}_q[\log p(\boldsymbol{\nu}, \mathbf{y})] - \mathbb{E}_q[\log q(\boldsymbol{\nu})]. \end{aligned} \quad (2)$$

The first term in (2) corresponds to the expected log joint distribution, while the second term is the entropy of the variational distribution.

A useful family of variational distributions employed to approximate  $p(\boldsymbol{\nu} | \mathbf{y})$  in Bayesian hierarchical models is the mean-field variational family, where  $q(\boldsymbol{\nu})$  is decoupled into “factors” that are independent of each other and each governed by a distinct variational parameter vector (also referred to as a “block” of parameters)  $\boldsymbol{\nu}_j$ :

$$q(\boldsymbol{\nu}) = \prod_j q(\boldsymbol{\nu}_j).$$

When used in the context of a conditionally-conjugate model specification, this factorization allows for closed-form updates which greatly enhance scalability via the use of coordinate ascent variational inference (CAVI). In CAVI, each factor is updated iteratively, maximizing the ELBO with respect to one block of variables  $\boldsymbol{\nu}_j$  at a time:

$$\log q(\boldsymbol{\nu}_j) = \mathbb{E}_{-j}[\log p(\mathbf{y}, \boldsymbol{\nu})] + \text{cst},$$

where cst is a normalization constant. Here, the notation  $\mathbb{E}_{-j}[\cdot]$  denotes the expectation over all factors

$q(\nu_i)$  with  $i \neq j$ .

Based on the posterior decomposition of Bayesian hierarchical models (Formula 1), we adopt the following mean-field factorization of the variational distribution natural arises:

$$q(\nu) = q(\nu^g) \prod_{t=1}^q q(\nu_t^l),$$

where each “local factor”  $q(\nu_t^l)$  reflects the variational approximation to the posterior  $p(\nu_t^l \mid \mathbf{y})$  of model unit  $t$ , while the “global factor”  $q(\nu^g)$  is an approximation to the posterior  $p(\nu^g \mid \mathbf{y})$ . Then the update of the local and global factors in each iteration are

$$\log q(\nu_t^l) = \mathbb{E}_{q(\nu_{-t}^l)q(\nu^g)}[\log p(\mathbf{y}, \nu)] + \text{cst}, \quad (3)$$

and

$$\log q(\nu^g) = \mathbb{E}_{q(\nu^l)}[\log p(\mathbf{y}, \nu)] + \text{cst}, \quad (4)$$

respectively. In this way, the CAVI algorithm alternates between updating each local factor  $q(\nu_t^l)$  while keeping all others fixed, and then updating the global variational factor  $q(\nu^g)$  conditional on the current local updates. This block-wise update strategy efficiently exploits the hierarchical model structure (see Algorithm 1).

---

**Algorithm 1** CAVI algorithm in the global-local framework

---

**Require:** Data  $\mathbf{y}$ ; model  $p(\mathbf{y}, \nu)$ .

- 1: Initialize  $\mathcal{L}(q) \leftarrow -\infty$ ; global and local variational factors  $q(\nu^g), q(\nu_t^l), t = 1, \dots, q$ ;
  - 2: **while**  $\mathcal{L}(q)$  has not converged **do**
  - 3:     **for**  $t = 1, \dots, q$  **do**
  - 4:         Update  $q(\nu_t^l)$  according to (3)
  - 5:     **end for**
  - 6:     Update  $q(\nu^g)$  according to (4)
  - 7: **end while**
  - 8: **return**  $q(\nu^g), q(\nu_t^l), t = 1, \dots, q$ .
- 

### 3 The adaptive focus strategy for CAVI

High-dimensional Bayesian hierarchical models often use sparse priors, such as spike-and-slab [12] and horseshoe priors [13], to shrink irrelevant parameters to zero. In the context of CAVI, each update corresponds to a partial maximization of the ELBO, i.e., maximization with respect to the variational parameter under consideration, while keeping others fixed. In high-dimensional settings where the number of units is large, we propose incorporating a unit selection mechanism *directly as part of* the CAVI inference algorithm, leveraging the very nature of sparse modeling formulations. In broad terms, at each iteration  $i$ , we introduce a  $q$ -dimensional binary selection vector  $\mathbf{z}^{(i)}$  that identifies which units contribute the most to maximizing the ELBO. The corresponding subset of selected units  $\mathcal{T}^{(i)} \subset \{1, \dots, q\}$  then defines which local factors with  $t \in \mathcal{T}$  are updated, while the other local regression parameters are temporarily “stalled”. Specifically, each entry  $t \in \{1, \dots, q\}$  of the binary vector  $\mathbf{z}^{(i)}$  is drawn from a Bernoulli distribution with probability parameter  $\omega_t^{(i)}$  constructed based on the current “activity” status of the unit  $t$ , namely,

$$\omega_t^{(i)} = (1 - \varepsilon^{(i)}) + a_t^{(i)} \varepsilon^{(i)}, \quad t = 1, \dots, q, \quad (5)$$

where:

- $a_t^{(i)} \in [0, 1]$  is a model-dependent score conveying the current evidence for unit  $t$ 's activity (with larger values representing more support) based on parameter estimates obtained at iteration  $i$ ; an example in the context of a spike-and-slab model will be provided in Section 4.4.
- $\varepsilon^{(i)}$  is a stochastic perturbation parameter that decays from 1 to 0 during the course of the inference according to a prespecified schedule. This ensures that each response receives a sufficiently high activity score during the first iterations, so their corresponding local parameters have high probability of getting updated at the early exploration stages of the posterior space, before progressively and adaptively focusing on the active ones. Examples of possible schedules, and their impact on inference, will be evaluated and discussed in Section 4.4.

We hereafter refer to this procedure as an ‘‘adaptive focus strategy’’ for CAVI, *AF-CAVI* (Algorithm 2).

---

**Algorithm 2** AF-CAVI algorithm in the global-local framework

---

**Require:** Data  $\mathbf{y}$ ; model  $p(\mathbf{y}, \boldsymbol{\nu})$ .

- 1: Initialize  $\mathcal{L}(q) \leftarrow -\infty$ ; global and local variational factors  $q(\boldsymbol{\nu}^g), q(\boldsymbol{\nu}_t^l), t = 1, \dots, q$ ; Iteration  $i = 0$ ;
  - 2: **while**  $\mathcal{L}(q)$  converge **do**
  - 3:      $i = i + 1$
  - 4:     Draw subset  $\mathcal{T}^{(i)} \subset \{1, \dots, q\}$  with adaptive activity scores  $\boldsymbol{\omega}^{(i)} = (\omega_1^{(i)}, \dots, \omega_q^{(i)})$ .
  - 5:     **for**  $t \in \mathcal{T}$  **do**
  - 6:         Update  $q(\boldsymbol{\nu}_t^l)$  according to (3)
  - 7:     **end for**
  - 8:     Update  $q(\boldsymbol{\nu}^g)$  according to (4)
  - 9: **end while**
  - 10: **return**  $q(\boldsymbol{\nu}^g), q(\boldsymbol{\nu}_t^l), t = 1, \dots, q$ .
- 

## 4 Assessment of AF-CAVI

### 4.1 Motivating example

With the Olink immuno assay technology [14] that allows for measuring thousands of plasma proteins simultaneously, the UK Biobank Pharma Proteomics Project (UKB-PPP) provides measurements for nearly 3 000 unique proteins of over 50 000 UK Biobank participants [15]. These participants were genotyped at about 850 000 variants and data of over 90 million imputed variants were also made available [3]. This resource provides a good test case for showing how our AF-CAVI algorithm can reduce the cost of applying Bayesian hierarchical models to large and high-dimensional data. In this study, we use the UKB-PPP data of  $n = 36\,626$  white British individuals and their  $q = 2\,919$  protein measurements. The sample, proteomic and genetic data quality control filters applied are detailed in Appendix C. In Section 4.5, we use real proteomic levels from the UKB-PPP dataset. In Section 4.4, we simulate proteomic responses from real single nucleotide polymorphisms (SNPs) on chromosome 19 filtered after quality control.

Here we apply the atlasQTL model [16] for joint pQTL mapping. Considering each response (here trait indexed by ‘ $t$ ’) in QTL mapping as a unit, atlasQTL constructs a local regression between each of the  $q$  responses  $\mathbf{y}_t$  and  $p$  candidate predictors (here SNPs indexed by ‘ $s$ ’)  $\mathbf{X} = (\mathbf{X}_1, \dots, \mathbf{X}_p)$ :

$$\mathbf{y}_t \mid \boldsymbol{\beta}_t, \tau_t \sim N_n(\mathbf{X}\boldsymbol{\beta}_t, \tau_t^{-1}\mathbf{I}_n), \quad t = 1, \dots, q,$$

where  $\beta_t$  and  $\tau_t$  are local parameters corresponding to the regression coefficient vector and residual precision parameter of each regression, respectively. As a typical choice in sparse hierarchical regressions, atlasQTL assigns a spike-and-slab prior to the regression coefficient  $\beta_{st}$  corresponding to the association between each predictor  $s$  and response  $t$ :

$$\beta_{st} \mid \gamma_{st}, \tau_t, \sigma \sim \gamma_{st} N(0, \sigma^2 \tau_t^{-1}) + (1 - \gamma_{st}) \delta_0, \quad s = 1, \dots, p,$$

where  $\delta_0$  is the delta Dirac distribution at zero, representing null effects, and  $\sigma^2$  is a global parameter corresponding to the prior signal-to-noise ratio. Moreover, parameter  $\gamma_{st}$  is a binary local parameter defining whether an association exists. It is further assigned a Bernoulli prior whose success probability depends on a global “hotspot propensity” parameter that is shared across regressions, thereby flexibly pooling information across them through the model hierarchy (see Appendix A for the full model).

One main goal of inference is to estimate the posterior probabilities of association between each SNP  $s$  and each trait  $t$ , i.e., the posterior probabilities of inclusion (PPI)

$$p(\gamma_{st} = 1 \mid \mathbf{y}) = \mathbb{E}(\gamma_{st} \mid \mathbf{y}), \quad (6)$$

which can be used to perform variable selection [17]. However, inferring the updates for  $\gamma_{st}$  and  $\beta_{st}$  represents a substantial computational burden as it requires expensive matrix multiplications. By limiting these updates to a small subset of indices at each iteration, the adaptive focus strategy should therefore be effective in alleviating this burden. A key component of the AF-CAVI strategy is the definition of the *activity score*  $a_t^{(i)}$ , which quantifies the relevance of each trait (or “unit”)  $t$  at each iteration  $i$  (see (5)). Here, the posterior probability that trait  $t$  is associated with at least one SNP, as estimated at iteration  $i$ , forms a natural score,

$$a_t^{(i)} = p^{(i)} \left( \sum_{s=1}^p \gamma_{st} > 0 \mid \mathbf{y} \right). \quad (7)$$

## 4.2 Data simulation

To emulate real settings whereby genotyping data entail local correlation patterns (linkage disequilibrium, LD), we use observed SNPs and simulate proteomic responses based on the data generation functions available from the R package `echoseq` [16]. The data generation procedure involves three steps. First, for a genomic region involving  $p$  SNPs (“block”), we select a percentage  $a_p$  of “active” SNPs (i.e., SNPs associated with at least one protein) and a percentage  $a_q$  of active proteomic responses (i.e., protein associated with at least one SNP), and define their association structure as follows. For each active SNP  $s$ , we generate a *propensity parameter* (i.e., the higher the propensity of SNP  $s$ , the stronger its likelihood of being linked to multiple responses) from a Beta(1, 5) distribution. Varying propensity parameters generate SNPs associated with different numbers of active responses. This right-skewed distribution ensures most SNPs are associated with only a few proteins, while allowing a small number of SNPs to be associated with many proteins (i.e., to be “hotspots”).

Next, active responses are generated using an Gaussian linear additive model (i.e., each copy of the minor allele leads to a linear increase in risk). Each regression coefficient  $\beta_{st}$  is implicitly obtained from a chosen SNP-specific heritability  $h_{st}^2$ , defined in a narrow-sense as the proportion of variance in response  $t$  explained by SNP  $s$ . Here we first select an *average total heritability level*  $h_m^2$ , and generate response-specific total heritability levels (i.e., variance in response  $t$  explained by all its associated SNPs)  $h_t^2$ ,  $t = 1, \dots, q$ , from Beta  $(1, (1 - h_m^2)/h_m^2)$ . Then, for each SNP  $s = 1, \dots, p$ , we sample  $h_{st}^2$  from a

Beta(2, 5) distribution, which ensures that most active SNPs have small effects, while a few of them have large effects. We then rescale the  $h_{1t}^2, \dots, h_{pt}^2$  so that  $\sum_{s=1}^p h_{st}^2 = h_t^2$ .

Finally, to mimic realistic settings whereby the residuals exhibit correlation across traits (i.e., not accounted for by the available genetic data), we simulate the responses with noise that exhibits equicorrelation  $\rho \in (0, 0.5)$  within groups of 50 traits. Details of the simulation procedure are given in Appendix B.

### 4.3 A toy example

Before comparing the performance of AF-CAVI to the vanilla version of CAVI, we present a toy simulation that demonstrates the advantage of Bayesian hierarchical modeling for molecular QTL mapping, over conventional univariate testing. To limit the computational burden under the vanilla algorithm, we choose a relatively small dataset, with  $p = 200$  consecutive SNPs on chromosome 19,  $n = 36\,626$  individuals. We then simulate associations for a single active SNP with 200 responses out of  $q = 1000$  responses in total; this SNP therefore constitutes a hotspot. We also set a very low percentage of variance explained by the single SNP of  $h_m^2 = 0.05\%$  to simulate a challenging scenario with a large number of weak association signals. We then compare the statistical performance of univariate screening (using the `glm` function in PLINK2) and atlasQTL with vanilla CAVI. To mitigate method-specific discrepancies caused by the differences in handling proxy signals due to the LD structure, we treat the 200 SNPs as a single locus and summarize the output of each method by taking the minimum  $p$ -value across all SNPs for each response in the univariate case, and the maximum PPI for atlasQTL. The corresponding Receiver Operating Characteristic (ROC) and Precision Recall (PR) curves shown in Figure 1 indicate that atlasQTL (AUROC 0.932 and AUPRC 0.891) largely outperforms univariate screening (AUROC 0.855 and AUPRC 0.768). This demonstrates the increased power of multivariate Bayesian methods which share information across co-regulated proteins to enhance the detection of weak pQTL signals. This observation has been extensively validated by Ruffieux, Davison, Hager, et al. [16] in their evaluation of the atlasQTL model, as well as in other Bayesian QTL mapping models [17–19].

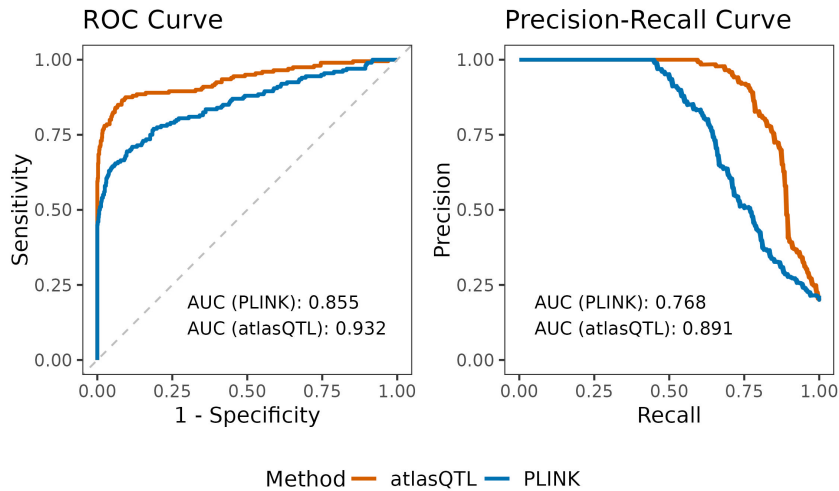


**Figure 1: Comparison of ROC (left) and PR (right) curves for atlasQTL and univariate testing in a toy example.** Scenario with many weak association signals emulating the genetic basis of complex traits: here a single active SNP (out of 200) is associated with 200 proteins (out of 1000) and the average trait heritability for the active proteins is 0.05%.

#### 4.4 Assessment of AF-CAVI in simulated data

In this section, we evaluate the computational and statistical performance of our proposed algorithm AF-CAVI for the atlasQTL model, comparing it with the vanilla CAVI implementation. To this end, we simulate data with the same sample size as that of the UKB-PPP dataset, namely  $n = 36\,626$  individuals, and generate  $p = 1\,000$  candidate predictors and  $q = 3\,000$  responses, following the procedure described in Section 4.2. According to the Framingham Heart Study [20] ( $n = 5\,626$ ), the average heritability of the whole blood transcriptome is 0.13 with 10% display heritability  $> 0.2$ . Therefore, we use a reference simulation scenario with average heritability of  $h_m^2 = 0.15$ , which we complete with two additional scenarios with lower ( $h_m^2 = 0.05$ ) and higher ( $h_m^2 = 0.3$ ) heritability levels. As the pilot pQTL study with univariate screening [4] shows that the majority (62.1%) of active loci are associated with a single protein (the 5<sup>th</sup> and 95<sup>th</sup> quantiles of the distribution of the number of proteins associated with active loci are 1 and 4, respectively), we set  $a_q = 0.005$  as the general sparse scenario (leading to 15 active proteins). We also simulate denser scenarios, namely with of  $a_q = 0.2$  (i.e., leading to 600 active proteins) and an extreme case of  $a_q = 0.5$ . Finally, we use  $a_p = 0.01$  in all simulation scenarios (i.e., leading to 10 active SNPs in total). Each scenario is simulated 50 times.

We compare AF-CAVI with the vanilla CAVI implementation, which updates all parameters at each iteration, as well as a *Randomly Focused CAVI (RF-CAVI)*, which randomly updates 50% of the local factors at each iteration. As outlined in Section 3, at iteration  $i$ , the local factors of trait  $t$  are updated with probability  $\omega_t^{(i)}$  according to (5), with the model-specific activity score  $a_t^{(i)}$  defined in (7). Here we compare two schemes for the stochastic perturbation parameter schedule:

- the *ELBO-scheme AF-CAVI (AFE-CAVI)*:  $\varepsilon^{(i)}$  is based on the difference in ELBO, using a logistic decay:

$$\varepsilon^{(i)} = \frac{1}{1 + \exp[-\log \Delta \mathcal{L}^{(i)}(q)]},$$

where  $\Delta \mathcal{L}^{(i)}(q) = \mathcal{L}^{(i-1)}(q) - \mathcal{L}^{(i-2)}(q)$  is the difference of ELBO in the previous two iterations.

- the *iteration-scheme AF-CAVI (AFI-CAVI)*:  $\varepsilon^{(i)}$  decays deterministically with each iteration as:

$$\varepsilon^{(i)} = 0.95^{i-1}.$$

Note that in the AFI-CAVI scheme, the ELBO does not need to be calculated in each iteration. Thus we implement an additional scheme:

- the *iteration-scheme optimized CAVI (AFIO-CAVI)*, where we further reduce the computational cost by computing the ELBO to assess convergence only intermittently, increasing the frequency of its evaluations as the improvement in ELBO diminishes, thus minimizing overhead while maintaining effective convergence monitoring.

To ensure sufficient exploration in the early stage of the algorithm, in RF-CAVI and all AF-CAVI schemes, we first update all local factors for the initial 50 iterations. Following Ruffieux, Davison, Hager, et al. [16], an annealing procedure is also added in this initialization stage (via a regularization of the entropy term in (2)), which improves the exploration of the parameter space, mitigating the risk of entrapment in local modes.

The computational efficiency of these approaches is evaluated using relative performance metrics, defined as the percentage change in a given metric when comparing a given approach to the baseline



vanilla CAVI. These metrics are formally expressed as:

$$\Delta\text{metric} (\%) = \frac{\text{metric}_{\text{method}} - \text{metric}_{\text{Vanilla}}}{\text{metric}_{\text{Vanilla}}} \times 100 \quad (8)$$

In particular, we evaluate two key metrics: (i) the reduction in runtime, denoted as  $\Delta\text{runtime}$ , which quantifies the efficiency gain in terms of execution time, and (ii) the relative change in the total number of iterations, denoted as  $\Delta\text{iterations}$ , which captures the reduction or increase in convergence steps required by the method.

For one iteration of the vanilla CAVI, updating local factors takes on average 74.5% of the per-iteration runtime, while the updates of global factors and ELBO takes 15.2% and 10.3% respectively. Therefore, in addition to reporting the overall runtime reduction ( $\Delta\text{runtime} (\text{total})$ ), we also quantify the reduction in runtime specifically attributed to local factor updates ( $\Delta\text{runtime} (\text{local})$ ) to offer a more granular view of the performance gains (Figure 2). We also report the statistical performance of each approach, in terms of precision, recall and false positive rate (FPR). These metrics were selected with a focus on the capability to identify true associations while controlling false discoveries, considering the high sparsity of the problem.

For all methods, the precision, recall, FPR and ELBO at convergence show little differences compared to the vanilla CAVI (see Table 1 for results in  $h_m^2 = 0.15$  and  $a_q = 0.005$ , see Appendix D for results in other simulation scenarios). However, adaptive focus methods significantly outperform RF-CAVI achieving greater runtime reduction with very marginal increase in the number of iterations. This highlights the ability of the adaptive focus strategy in making an effective parsimonious choice as of which local factors to update. Among all the adaptive focus schemes, AFIO-CAVI demonstrates the highest reduction in runtime, achieving about 75% reduction in the local factors and 50% in total runtime in the general sparse scenario ( $a_q = 0.005$ ). A comparison across different  $a_q$  levels shows that the adaptive focus strategy has higher potential in runtime reduction for problems with higher sparsity (i.e., lower  $a_q$ ). This finding is consistent across different heritability levels (Appendix D). While the best-performing AF-CAVI scheme may vary across different models and applications, the consistent patterns observed here suggest that the advantage of adaptively focusing updates is broadly generalizable. Hereafter, we will use our best-performing scheme, the AFIO-CAVI, for the rest of the paper. The algorithm is implemented in a stand-alone R package called `AFatlasQTL`.

#### 4.5 Assessment of AF-CAVI on pQTL discovery on CHR19

We now assess the performance of AF-CAVI in conducting genome-wide joint pQTL mapping on a real data problem. To this end, we use the pipeline described in Figure 3 which involves an application of the atlasQTL implementation of AF-CAVI (using the best-performing, AFIO-CAVI scheme). To allow for parallel running, we divide the entire chromosome into approximately LD-independent blocks with boundaries inferred by LDetect [21] using the 1000 Genomes Phase 1 Reference panel. This results in a partition of 39 blocks, each containing between 1 000 and 2 000 SNPs after quality control (Appendix E). For each block, the 2 919 proteomic responses are modeled jointly. As for the toy example, to mitigate any irrelevant differences arising from proxy signals due to LD, we summarize the results “locus-wise” by merging signals within a distance of 0.5 Mb. We use a threshold on the PPI of 0.5 to report signals, following to the median probability model rule of [22]. Starting from the SNP with the largest number of associated proteins on the block, any signals within a 0.5 Mb distance of this SNP are considered part of the same locus. The same process is repeated for the next unassigned SNP with the largest number

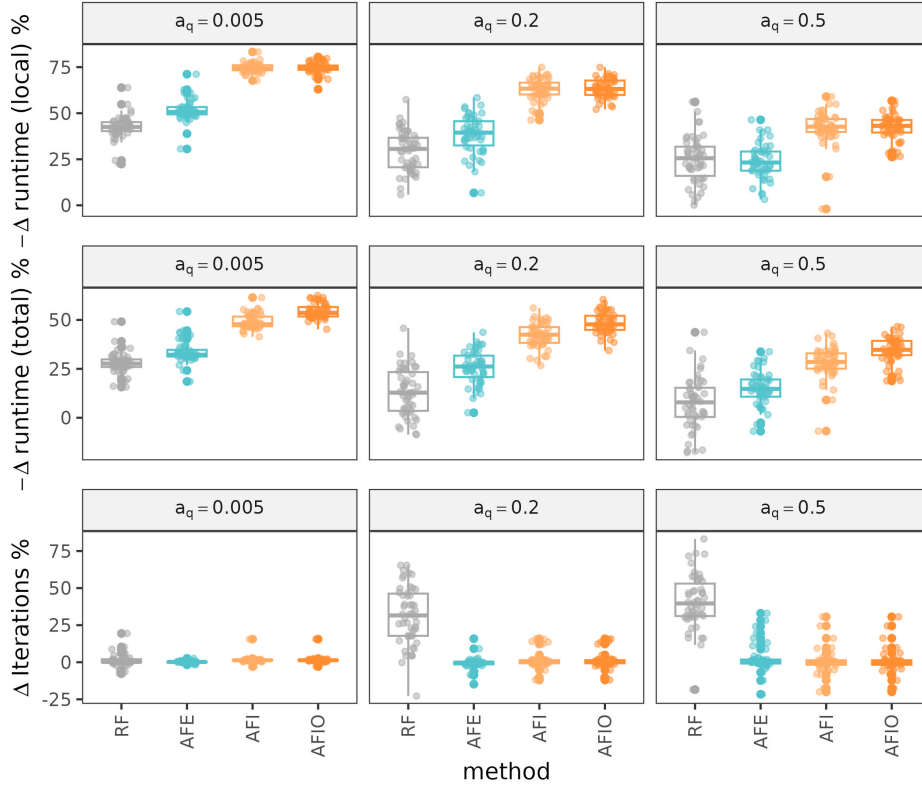


**Figure 2: Relative differences in runtime (local and total) and iterations for the RF-CAVI and series of AF-CAVI algorithms, with respect to the vanilla CAVI for problems with various sparsity levels.** Problems are with average heritability  $h_m^2 = 0.15$  and sparsity  $a_q \in \{0.005, 0.2, 0.5\}$  (columns). The relative performance metrics employed are defined in (8). See Appendix D for results in other simulation scenarios.

of associated proteins until all are assigned. Finally, a list of loci with associated proteins is reported (Figure 3). To demonstrate this procedure, we select 6 blocks across chromosome 19 for which we compare AF-CAVI to the vanilla and AF-CAVI. The problems corresponding to these blocks were found to reflect different sparsity levels according to UK Biobank pilot pQTL study.

On an Intel Xeon Platinum 8276 2.2 GHz machine, the adaptive focus strategy reduced the runtime by roughly 50%, which is in line with the simulation results of Section 4.4. It also required on average 6 GB of peak memory usage (Table 2). The pQTL loci and their associated proteins identified with the vanilla and AF-CAVI are identical (Table 3), and the PPIs and regression parameter estimates for reported signals (maximum value for each protein in the loci in Figure 4) are also nearly indistinguishable. Such results further confirm the capability of AF-CAVI to reduce the computational cost of Bayesian modeling while preserving statistical performance in biobank-scale analysis.

## 5 Discussion

Motivated by the computational demands in biobank-scale analysis, we have introduced an *adaptive focus strategy* for VI, AF-CAVI, tailored to large Bayesian hierarchical models. AF-CAVI prioritizes updating local variational factors corresponding to units whose “activity” is supported by the data as the algorithm progresses. This results in a probabilistic framework involving *activity scores* which are dynamically updated to ensure both convergence and thorough exploration of the parameter space.

Method	FPR ( $\times 10^{-6}$ )	Precision	Recall
Vanilla	$3.53 \pm 0.30$	$0.73 \pm 0.02$	$0.93 \pm 0.01$
RF	$3.93 \pm 0.34$	$0.71 \pm 0.02$	$0.93 \pm 0.01$
AFE	$3.54 \pm 0.30$	$0.73 \pm 0.02$	$0.93 \pm 0.01$
AFI	$3.51 \pm 0.30$	$0.73 \pm 0.02$	$0.93 \pm 0.01$
AFIO	$3.51 \pm 0.30$	$0.73 \pm 0.02$	$0.93 \pm 0.01$

**Table 1: Comparison of FPR, precision and recall of the different CAVI implementations in the reference simulation scenario** ( $h_m^2 = 0.15$ ,  $a_q = 0.005$ ). Average metrics are reported with  $\pm$  standard error computed across 50 replicates. See Appendix D for results in other simulation scenarios.

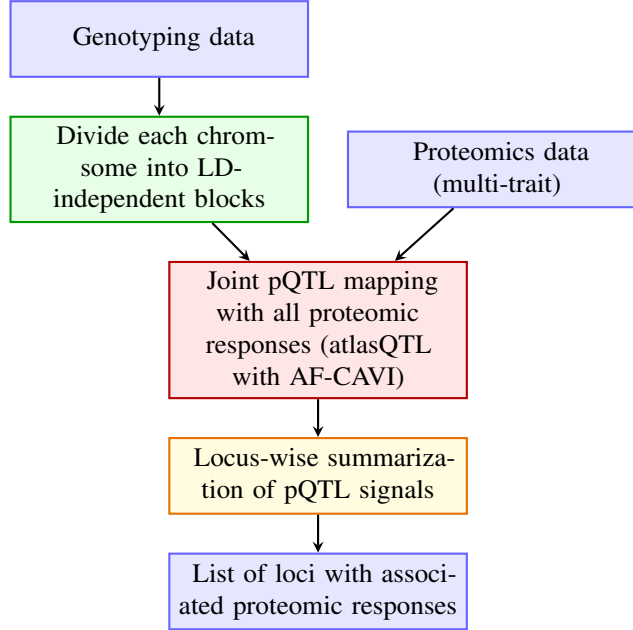


**Figure 3: Pipeline for genome-wide joint pQTL mapping using the AF-CAVI algorithm for the atlasQTL model [16].**

To assess the ability of the adaptive focus strategy to reduce the runtime without sacrificing statistical performance, we conducted pQTL mapping in the UKB-PPP data, implementing the AF-CAVI algorithm for the atlasQTL model, which is tailored to multi-response joint QTL analysis. In simulated data emulating the genetic basis of 3 000 proteins, (which corresponds to the current scale of the UKB-PPP datasets), our best-performing AF-CAVI scheme achieves up to 75% runtime reduction in updating local factors and 50% total runtime reduction in the general sparse scenario, with precision, recall and FPR virtually unchanged compared to the vanilla CAVI algorithm. Our comparisons with the RF-CAVI scheme – which updates random subsets of local factors – further showed the advantage of the adaptive focus strategy in reducing the runtime per iteration while controlling the number of iterations needed for convergence. The computational and statistical performance of AF-CAVI were also supported by comparisons with the vanilla CAVI on the real UKB-PPP data. In fact, by dividing the chromosome into LD-independent blocks, multi-response pQTL mapping on each block can be run on different CPUs in parallel.

Our adaptive focus strategy differs from the stochastic CAVI proposed by Hoffman, Blei, Wang, et al. [23], which is limited to global-local models where each local factor corresponds to an individual sample. In stochastic CAVI, a random subset of samples is selected at each iteration to update the corresponding local factor. In contrast, our AF-CAVI algorithm is designed for a broader class of global-local models where each variational factor corresponds to a model unit. In addition, we have introduced a stochastic

block ID	block start (bp)	block end (bp)	p	Runtime (min)		Iterations		Memory (GB)
				Vanilla CAVI	AF-CAVI	Vanilla CAVI	AF-CAVI	
3	2098397	3019660	1216	33.61	16.01	516	522	5.77
8	8347514	9238393	746	12.65	7.26	364	372	4.74
17	20905758	22732896	1148	29.12	13.69	490	496	5.70
28	40984602	42131573	1046	24.82	12.68	467	473	6.09
30	43862456	44744108	704	11.41	6.73	350	356	4.59
37	54602363	55728080	1585	74.32	41.89	607	610	6.81

**Table 2: Comparison of runtime, number of iterations and peak running memory usage between the vanilla CAVI and AF-CAVI on selective blocks of chromosome 19.** The peak memory usage of both methods are identical and thus only one column is shown.

Locus ID	Locus start (bp)	Locus end (bp)	# of <i>cis</i> signals	# of <i>trans</i> signals
1	2404384	2917689	2	
2	8366982	8785951	2	
3	41249427	42131442	8	
4	43864016	44649737	9	
5	55028894	55725410	27	
6	54603173	55025911	16	
7	40986303	41204986	1	
8	8941342	9140207	1	
9	44657909	44716079	3	
10	21126762	21155558	0	
11	22133293	22717170	0	
12	2109157	2239966	0	

**Table 3: Summary of associated proteins in each locus reported by atlasQTL.** The results for the vanilla CAVI and AF-CAVI algorithms are identical. *cis* pQTLs are within  $\pm 1$  Mb of the protein’s gene position and *trans* are outside this window.

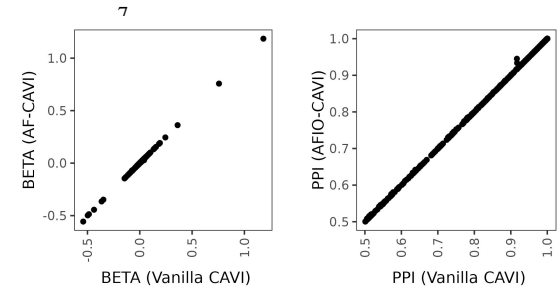


**Figure 4: Regression coefficients (a.k.a. BETA, left) and PPI (right) inferred by the vanilla CAVI and AF-CAVI algorithms in each locus.** Maximum value is taken for each response in each locus.

perturbation mechanism in the selection of local factors, which shares similarity with the adaptive scanning MCMC suggested in Richardson, Bottolo, and Rosenthal [24] for sparse Bayesian hierarchical regressions. Such ideas have also been discussed in the context of convex optimization. Random Adaptive Coordinate Decent Method (RACDM) proposed by Nesterov [25] implements updates along a single coordinate direction instead of the full gradient, which is selected according to a probability distribution that can be adapted to reflect the local geometry of the objective function, typically based on the Lipschitz constants of the partial derivatives.

The computational efficiency gains achieved by AF-CAVI will vary according to the model and data at hand, particularly depending on the level of sparsity. The atlasQTL multi-trait pQTL mapping example is a general family of hierarchically linked sparse regressions, which are widely applied for association estimation. We also anticipate AF-CAVI to be an efficient tool for network models based on spike-and-slab priors, useful to study gene co-expression structures, especially in settings where edges are sparsely distributed.

In summary, our proposed AF-CAVI method bridges the gap between the flexibility of Bayesian joint modeling for sparse problems and the computational demands inherent in large-scale, high-dimensional real-world analyses. Our framework is general and can be extended to a wide range of structured inference problems. Its computational efficiency positions it as a powerful tool, enabling effective applications of Bayesian models to complex, genome-wide biobank-scale analyses, and pushing the boundaries of statistical genetics and genomics.

## **6 Software availability**

The proposed AF-CAVI method for atlasQTL is implemented in an open-source R package `AFatlasQTL`, available at <https://github.com/yiran2000/AFatlasqtl>.

## **7 Funding information**

This work was funded by UKRI Programme Grant MC\_UU\_00040/01, and supported by the Lopez–Loreta Foundation (H.R.). For the purpose of open access, the authors have applied a Creative Commons Attribution (CC BY) license to any Author Accepted Manuscript version arising.

## **8 Acknowledgments**

This research has been conducted using the UK Biobank Resource under application number 98032. We thank Colin Starr for his valuable assistance with the algorithmic and R package development, as well as Prof. Adam Butterworth and Dr. Paul Lyons for their helpful insights and discussions.

## References

- [1] William Ollier, Sprosen Tim, et al. “UK Biobank: From Concept to Reality”. In: *Pharmacogenomics* 6.6 (Sept. 2005), pp. 639–646. DOI: 10.2217/14622416.6.6.639.
- [2] Wei Zhou, Masahiro Kanai, Kuan-Han H. Wu, et al. “Global Biobank Meta-analysis Initiative: Powering genetic discovery across human disease”. In: *Cell Genomics* 2.10 (Oct. 2022). DOI: 10.1016/j.xgen.2022.100192.
- [3] Clare Bycroft, Colin Freeman, Desislava Petkova, et al. “The UK Biobank resource with deep phenotyping and genomic data”. en. In: *Nature* 562.7726 (Oct. 2018), pp. 203–209. DOI: 10.1038/s41586-018-0579-z.
- [4] Benjamin B. Sun, Joshua Chiou, Matthew Traylor, et al. “Plasma proteomic associations with genetics and health in the UK Biobank”. en. In: *Nature* 622.7982 (Oct. 2023), pp. 329–338. DOI: 10.1038/s41586-023-06592-6.
- [5] Karsten Suhre. “Genetic associations with ratios between protein levels detect new pQTLs and reveal protein-protein interactions”. English. In: *Cell Genomics* 4.3 (Mar. 2024). DOI: 10.1016/j.xgen.2024.100506.
- [6] Mihir G. Sukhatme, Asha Kar, Uma Thanigai Arasu, et al. *Integration of single cell omics with biobank data discovers trans effects of SREBF1 abdominal obesity risk variants on adipocyte expression of more than 100 genes*. en. Nov. 2024. DOI: 10.1101/2024.11.22.24317804.
- [7] Ruiyan Luo and Hongyu Zhao. “Bayesian hierarchical modeling for signaling pathway inference from single cell interventional data”. In: *The annals of applied statistics* 5.2A (2011), pp. 725–745. DOI: 10.1214/10-AOAS425.
- [8] Samprit Banerjee, Brian S. Yandell, and Nengjun Yi. “Bayesian Quantitative Trait Loci Mapping for Multiple Traits”. en. In: *Genetics* 179.4 (Aug. 2008), p. 2275. DOI: 10.1534/genetics.108.088427.
- [9] Timothée Flutre, Xiaoquan Wen, Jonathan Pritchard, et al. “A Statistical Framework for Joint eQTL Analysis in Multiple Tissues”. en. In: *PLOS Genetics* 9.5 (May 2013), e1003486. DOI: 10.1371/journal.pgen.1003486.
- [10] Youshu Cheng, Biao Cai, Hongyu Li, et al. “HBI: a hierarchical Bayesian interaction model to estimate cell-type-specific methylation quantitative trait loci incorporating priors from cell-sorted bisulfite sequencing data”. In: *Genome Biology* 25.1 (Oct. 2024), p. 273. DOI: 10.1186/s13059-024-03411-7.
- [11] David M. Blei, Alp Kucukelbir, and Jon D. McAuliffe. “Variational Inference: A Review for Statisticians”. en. In: *Journal of the American Statistical Association* 112.518 (Apr. 2017), pp. 859–877. DOI: 10.1080/01621459.2017.1285773.
- [12] Hemant Ishwaran and J. Sunil Rao. “Spike and slab variable selection: Frequentist and Bayesian strategies”. In: *The Annals of Statistics* 33.2 (Apr. 2005), pp. 730–773. DOI: 10.1214/009053604000001147.
- [13] Carlos M. Carvalho, Nicholas G. Polson, and James G. Scott. “The horseshoe estimator for sparse signals”. en. In: *Biometrika* 97.2 (2010), pp. 465–480.
- [14] Erika Assarsson, Martin Lundberg, Göran Holmquist, et al. “Homogenous 96-Plex PEA Immunoassay Exhibiting High Sensitivity, Specificity, and Excellent Scalability”. en. In: *PLoS ONE* 9.4 (Apr. 2014). Ed. by Jörg D. Hoheisel, e95192. DOI: 10.1371/journal.pone.0095192.

- [15] Benjamin B. Sun, Joshua Chiou, Matthew Traylor, et al. *Genetic regulation of the human plasma proteome in 54,306 UK Biobank participants*. en. June 2022. DOI: 10.1101/2022.06.17.496443.
- [16] H  l  ne Ruffieux, Anthony C. Davison, J  rg Hager, et al. “A global-local approach for detecting hotspots in multiple-response regression”. en. In: *The Annals of Applied Statistics* 14.2 (June 2020). DOI: 10.1214/20-AOAS1332.
- [17] Helene Ruffieux, Anthony C. Davison, Jorg Hager, et al. “Efficient inference for genetic association studies with multiple outcomes”. In: *Biostatistics* 18.4 (Oct. 2017), pp. 618–636. DOI: 10.1093/biostatistics/kxx007.
- [18] Marie Pier Scott-Boyer, Gregory C. Imholte, Arafat Tayeb, et al. “An Integrated Hierarchical Bayesian Model for Multivariate eQTL Mapping”. en. In: *Statistical Applications in Genetics and Molecular Biology* 11.4 (Jan. 2012). DOI: 10.1515/1544-6115.1760.
- [19] Kathryn E. Kemper, Philip J. Bowman, Benjamin J. Hayes, et al. “A multi-trait Bayesian method for mapping QTL and genomic prediction”. In: *Genetics Selection Evolution* 50.1 (Mar. 2018), p. 10. DOI: 10.1186/s12711-018-0377-y.
- [20] Tianxiao Huan, Chunyu Liu, Roby Joehanes, et al. “A Systematic Heritability Analysis of the Human Whole Blood Transcriptome”. In: *Human genetics* 134.3 (Mar. 2015), pp. 343–358. DOI: 10.1007/s00439-014-1524-3.
- [21] Tomaz Berisa and Joseph K. Pickrell. “Approximately independent linkage disequilibrium blocks in human populations”. In: *Bioinformatics* 32.2 (Jan. 2016), pp. 283–285. DOI: 10.1093/bioinformatics/btv546.
- [22] Maria M. Barbieri, James O. Berger, Edward I. George, et al. “The Median Probability Model and Correlated Variables”. en. In: *Bayesian Analysis* 16.4 (Dec. 2021). DOI: 10.1214/20-BA1249.
- [23] Matthew D Hoffman, David M. Blei, Chong Wang, et al. “Stochastic Variational Inference”. en. In: *Journal of Machine Learning Research* 14 (2013), pp. 1303–1347.
- [24] Sylvia Richardson, Leonardo Bottolo, and Jeffrey S. Rosenthal. “Bayesian Models for Sparse Regression Analysis of High Dimensional Data”. In: *Bayesian Statistics 9*. Ed. by Jos   M. Bernardo, M. J. Bayarri, James O. Berger, et al. Oxford University Press, Oct. 2011, p. 0. DOI: 10.1093/acprof:oso/9780199694587.003.0018.
- [25] Yu. Nesterov. “Efficiency of Coordinate Descent Methods on Huge-Scale Optimization Problems”. en. In: *SIAM Journal on Optimization* 22.2 (Jan. 2012), pp. 341–362. DOI: 10.1137/100802001.
- [26] H  l  ne Ruffieux, Anthony C. Davison, J  rg Hager, et al. “A global-local approach for detecting hotspots in multiple-response regression”. en. In: *The Annals of Applied Statistics* 14.2 (June 2020). DOI: 10.1214/20-AOAS1332.
- [27] Ruffieux Ruffieux. *ECHOSEQ R-package* (<https://github.com/hruffieux/echoseq>).
- [28] H  l  ne Ruffieux, J  r  me Carayol, Radu Popescu, et al. “A fully joint Bayesian quantitative trait locus mapping of human protein abundance in plasma”. en. In: *PLOS Computational Biology* 16.6 (June 2020), e1007882. DOI: 10.1371/journal.pcbi.1007882.
- [29] Ani Manichaikul, Josyf C. Mychaleckyj, Stephen S. Rich, et al. “Robust relationship inference in genome-wide association studies”. In: *Bioinformatics* 26.22 (Nov. 2010), pp. 2867–2873. DOI: 10.1093/bioinformatics/btq559.

# Appendices

## A Details of the atlaQTL model

Here we provide details of the atlasQTL model by Ruffieux, Davison, Hager, et al. [26]. Given  $p$  candidate predictors  $\mathbf{X} = (\mathbf{X}_1, \dots, \mathbf{X}_p)$  and  $q$  responses  $\mathbf{y} = (\mathbf{y}_1, \dots, \mathbf{y}_q)$ , atlasQTL constructs a series of hierarchically related regressions:

$$\begin{aligned} \mathbf{y}_t \mid \beta_t, \tau_t &\sim N_n(\mathbf{X}\beta_t, \tau_t^{-1}\mathbf{I}_n), \quad t = 1, \dots, q, \\ \beta_{st} \mid \gamma_{st}, \tau_t, \sigma &\sim \gamma_{st}N(0, \sigma^2\tau_t^{-1}) + (1 - \gamma_{st})\delta_0, \quad s = 1, \dots, p, \\ \gamma_{st} \mid \theta_s, \zeta_t &\sim \text{Bernoulli}\{\Phi(\theta_s + \zeta_t)\}, \quad \zeta_t \stackrel{\text{iid}}{\sim} N(n_0, t_0^2), \\ \theta_s \mid \lambda_s, \sigma_0 &\sim N(0, \lambda_s^2\sigma_0^2), \quad \lambda_s \stackrel{\text{iid}}{\sim} C^+(0, 1), \quad \sigma_0 \sim C^+(0, q^{-\frac{1}{2}}), \end{aligned}$$

where  $\delta_0$  is the Dirac distribution,  $\Phi(\cdot)$  is the standard normal cumulative distribution function, and  $C^+(\cdot, \cdot)$  is half-Cauchy distribution. The key parameters in this model are:

- $\beta_{st}$ : the regression coefficient between predictor  $\mathbf{X}_s$  and response  $\mathbf{y}_t$ ;
- $\gamma_{st}$ : a binary latent variable that takes value 1 when there is an association between  $\mathbf{X}_s$  and  $\mathbf{y}_t$  and 0 otherwise;
- $\theta_s$ : a hotspot propensity probability that controls the tendency of predictor  $\mathbf{X}_s$  to be associated with multiple responses;
- $\zeta_t$ : response specific parameter that adapts to the sparsity pattern corresponding to each response.

The model facilitates a joint modeling between predictors and responses in the way that each response,  $\mathbf{y}_t$ , is related linearly to the predictors  $\mathbf{X}$  with a specific precision  $\tau_t$ . The responses are conditionally independent across the regressions, while their dependence structure is captured via shared parameters  $\sigma^2$  and  $\theta_s$ , which are common to all the responses. Besides,  $\zeta_t$  is shared across predictors. This naturally serves co-selection of predictors and responses by leveraging strength across responses associated with the same predictors, as well as predictors associated with the same responses.

Sparsity is introduced at two levels. First,  $\beta_{st}$  is assigned a spike-and-slab prior, which puts all the mass at zero when  $\gamma_{st} = 0$ , and is normally distributed with mean 0 and variance  $\sigma^2\tau_t^{-1}$  when  $\gamma_{st} = 1$  ( $\sigma^{-2}$  and  $\tau_t$  are assigned Gamma priors). Tailored for hotspot detection, a hierarchical structure is further added to  $\gamma_{st}$ , which reflects both the propensity of  $\mathbf{y}_t$  to be associated with predictors (modeled by  $\zeta_t$ ), and propensity of  $\mathbf{X}_s$  to be associated with responses (modeled by  $\theta_s$ ). Then  $\theta_s$  is assigned a horseshoe prior, assuming the vast majority of predictors are not associated with any responses. With a pole at zero and a heavy, Cauchy-like tail controlled by  $\lambda_s^2\sigma_0^2$ , the horseshoe prior pushes most  $\theta_s$  to values close to zero while maintaining the capability to detect a few large signals. The global scale parameter  $\sigma_0$  controls the overall sparsity level and has a half-Cauchy prior with scale parameter  $q^{-1/2}$ , to increase pulling towards zero in large response settings thereby controlling for multiplicity (see [16]); the local parameter  $\lambda_s$  allows capturing the few large hotspot effects. Finally,  $\zeta_t$ , the parameter that sets the overall sparsity pattern of responses, has a normal distributed prior with mean  $n_0$  and variance  $t_0^2$  that are set to match the expectation and variance of the prior number of associated predictors per response.

Here we follow the default prior values, initializations and annealing schemes implemented by Ruffieux, Davison, Hager, et al. [26] in the R package `atlasqtl`. Prior of  $n_0$  and  $t_0$  are set to 1 and 4 respectively. The annealing temperature follows the default geometric schedule with initial temperature 2



with grid 10. The convergence tolerance, i.e., the difference of ELBO in two consecutive iterations for convergence is set to 0.01.

## B Data simulation strategies

Here we explain the details of generating additive responses  $\mathbf{y} = (\mathbf{y}_1, \dots, \mathbf{y}_q)$  from real SNPs  $\mathbf{X} = (\mathbf{X}_1, \dots, \mathbf{X}_p)$  according to

$$\mathbf{y}_t = \sum_{s=1}^p \beta_{st} \mathbf{X}_s + \boldsymbol{\varepsilon}_t, \quad t = 1, \dots, q. \quad (9)$$

Our simulation follows three steps:

1. Define the dependence structure  $\gamma_{st} = \mathbb{1}\{\mathbf{X}_s \text{ is associated with } \mathbf{y}_t\}$  for each pair of  $\mathbf{X}_s, \mathbf{y}_t$ ;
2. Simulate the error terms  $\boldsymbol{\varepsilon}_t$  with a specified correlation structure in the responses;
3. Simulate the effect sizes  $\beta_{st}$ .

The rest of this section explains the details of each step utilizing functions in the echoseq package [27] and parameters selected according to Ruffieux, Carayol, Popescu, et al. [28]. No missing value is inserted in the simulated responses for simplicity.

**Step 1: Defining the dependence structure** Randomly select  $a_p$  percentage of all SNPs to be “active”, i.e., associated with at least one response, while the other SNPs are set as “inactive” and not associated with any response. For each active predictor  $\mathbf{X}_s$ , we assign a propensity parameter:

$$\omega_s \sim \text{Beta}(1, 5),$$

which describes the probability of each active  $\mathbf{X}_s$  to be associated with any active  $\mathbf{y}_t$ . The propensity parameter follows a right-skewed Beta distribution that favors small values, so that most active SNPs are assigned only one associated protein, while a small fraction of active SNPs are hotspots. In the case that a response is not associated with any predictor, we randomly assign one response from the active set to be associated with this predictor. The same check is applied to all active responses.

**Step 2: Simulation of equicorrelated error terms** The correlation structure of responses is defined in a grouped fashion. We first group responses into  $B = \lceil q/s_q \rceil$  blocks of size  $s_q = 10$ . Responses within each block are equicorrelated with correlation  $\eta_b$  while those from different groups are independent. The correlation  $\eta_b$  of each block is uniformly distributed between 0 and 0.5, i.e.,

$$\eta_b \stackrel{\text{iid}}{\sim} \text{Unif}(0, 0.5), \quad b = 1, \dots, B.$$

The  $s_q \times s_q$  correlation matrix  $\boldsymbol{\Sigma}^{(b)}$  for responses in block  $b$  is then defined as:

$$\boldsymbol{\Sigma}_{ij}^{(b)} = \begin{cases} 1, & \text{if } i = j, \\ \eta_b, & \text{if } i \neq j, \end{cases}$$

In order to simulate the error terms  $\boldsymbol{\varepsilon}^{(b)} \sim N(0, \boldsymbol{\Sigma}^{(b)})$ , we perform Cholesky decomposition on  $\boldsymbol{\Sigma}^{(b)}$  such that  $\boldsymbol{\Sigma}^{(b)} = \mathbf{L}^{(b)} \mathbf{L}^{(b)T}$ . Let  $\mathbf{Z}^{(b)}$  be a  $n \times s_q$  matrix of  $s_q$  uncorrelated random variables normally

distributed with mean 0 and variance 1. Then

$$\boldsymbol{\varepsilon}^{(b)} = \mathbf{Z}^{(b)} \mathbf{L}^{(b)}.$$

follows a multivariate normal distribution with mean 0 and variance matrix  $\boldsymbol{\Sigma}^{(b)}$ .

**Step 3: Simulation of effect sizes** Effect sizes are simulated from, pre-defined heritability levels. By fitting a linear regression model considering only the additive effects as described in 9, the narrow-sense heritability (i.e., heritability solely due to the additive genetic effects, or the variance explained by  $\mathbf{X}$ ) for trait  $\mathbf{y}_t$  is

$$h_t^2 := \frac{\text{Var}(\mathbf{X}\boldsymbol{\beta}_t \mid \boldsymbol{\beta}_t)}{\text{Var}(\mathbf{y}_t)}.$$

Assuming uncorrelated predictors for simplification,  $h_t^2$  decomposes as a summarization of  $h_{st}^2$ , the variance of  $\mathbf{y}_t$  explained by each predictor  $\mathbf{X}_s$ :

$$h_t^2 = \sum_{s=1}^p h_{st}^2,$$

where

$$h_{st}^2 = \frac{\text{Var}(\mathbf{X}_s\boldsymbol{\beta}_{st} \mid \boldsymbol{\beta}_{st})}{\text{Var}(\mathbf{y}_t)} = \frac{\boldsymbol{\beta}_{st}^2 \text{Var}(\mathbf{X}_s)}{\text{Var}(\mathbf{y}_t)}.$$

We estimate  $\text{Var}(\mathbf{X}_s)$  empirically as

$$\widehat{\text{Var}}(\mathbf{X}_s) = 2f_s(1 - f_s),$$

where  $f_s$  denotes the empirical minor allele frequency (MAF) of  $\mathbf{X}_s$ . Further, we use  $\widehat{\text{Var}}(\mathbf{y}_t) = \widehat{\text{Var}}(\boldsymbol{\varepsilon}_t)/(1 - h_t^2)$ , where  $\widehat{\text{Var}}(\boldsymbol{\varepsilon}_t)$  is estimated empirically from our simulated values in Step 2, assuming genetic factors uncorrelated from environmental factors. Thus, given  $h_{st}^2$ ,  $\boldsymbol{\beta}_{st}$  can be derived as:

$$\boldsymbol{\beta}_{st} = \sqrt{\frac{h_{st}^2}{1 - h_t^2} \frac{\widehat{\text{Var}}(\boldsymbol{\varepsilon}_t)}{2f_s(1 - f_s)}}.$$

Therefore, one can simulate effect size  $\boldsymbol{\beta}_{st}$  by specifying the proportion of variance in  $\mathbf{y}_t$  explained by  $\mathbf{X}_s$ . Here we first select an *average heritability level*  $h_m^2$  for  $h_t^2$ , i.e.,

$$h_t^2 \sim \text{Beta}\left(1, \frac{1 - h_m^2}{h_m^2}\right).$$

This ensures that  $h_m^2$  is the expected total heritability of each response. Then for each  $t$ , We simulate  $h_{st}^2 \sim \text{Beta}(2, 5)$ , and rescale  $h_{1t}^2, \dots, h_{pt}^2$  such that their sum is  $h_t^2$ .

## C Quality control of the UKB-PPP data

The currently available UKB-PPP dataset contains 2 923 unique proteins measured for 53 021 participants at their initial assessment visit from 2006 to 2010. Genome-wide genotyping data is available for 52 567 participants. Measurements of their repeated assessments and COVID-19 repeat imaging study are not included in our study. We further limit our analysis to the 43 711 samples self-identified as white British and have similar genetic ancestry based on a principal components analysis of the genotypes. We then

removed 23 samples with likely sex swaps, and exclude 318 samples with duplicates or second-degree relations in the dataset (randomly excluded one sample from the 318 pairs of kinship coefficient over 0.1769 estimated by KING [29]). Noticing that 15.5% of the samples miss measurements on entire panels of cardiometabolic II, inflammation II, neurology II, and oncology II, we also remove such samples to avoid bias caused by missingness. Finally, we remove proteins with over 20% of missingness in the rest of the dataset, leaving  $q = 2\,919$  unique proteins and  $n = 36\,626$  samples. All the remaining samples have genotyping rate over 99%, and thus no further samples are removed.

Imputed genomic variants of UK Biobank are stored as “gene dosages”, which are triplets containing the probability of the variant containing two copies of the reference allele (homozygous reference genotype), one copy of the reference allele and one copy of the alternative allele (heterozygous genotype), or two copies of the alternative allele (homozygous alternative genotype). We translate gene dosages to a 0-2 scale during the additive dose-effect scheme, i.e.,

$$\hat{g}_{is} = E(g_{is}) = \mathbb{P}(g_{is} = 0) \times 0 + \mathbb{P}(g_{is} = 1) \times 1 + \mathbb{P}(g_{is} = 2) \times 2,$$

where  $\hat{g}_{is}$  denotes the (estimated) genotype for the  $s^{\text{th}}$  SNP of  $i^{\text{th}}$  sample, and 0, 1, 2 refer to the homozygous reference genotype, heterozygous genotype, homozygous alternative genotype respectively.

Within each block, we filter for high-quality imputed variants defined by: Info score  $> 0.8$ , MAF  $> 0.01$  (in the entire UK Biobank cohort), MAC  $> 20$  (in our QC-filtered samples), HWE exact test  $p$ -value  $> 10^{-15}$ , LD pruning with 1,000 variant windows, 100 sliding windows and  $r^2 < 0.9$ , and  $> 95\%$  of the expected gene dosage within 0.1 of either 0, 1 or 2. We select one block in chromosome 1 and one in 19 respectively, with the former (54 313 SNPs pruned to 1 071) being a region of few *trans*-pQTLs, while the later (82 945 SNPs pruned to 2 871) a likely hotspot according to the pQTL analysis of Sun, Chiou, Traylor, et al. [4].

We adjust the NPX values for age, age<sup>2</sup>, sex, age  $\times$  sex, age<sup>2</sup>  $\times$  sex, batch, UKB centre, UKB genetic array, time between blood sampling and measurement and the first 20 genetic PCs, and then conduct pQTL inference between on the regression residuals.

## D Simulation results in all scenarios

## E LD-independent blocks of chromosome 19 divided by LDetect

$h_m^2$	$a_q$	Method	$\Delta$ Iterations %	$-\Delta$ Runtime (total) %	$-\Delta$ Runtime (local) %	FPR ( $\times 10^{-4}$ )	Precision	Recall
0.05	0.005	Vanilla	NA	NA	NA	$0.04 \pm 0.00$	$0.68 \pm 0.01$	$0.89 \pm 0.01$
		RF	$-0.04 \pm 0.32$	$29.18 \pm 0.74$	$43.68 \pm 0.65$	$0.04 \pm 0.00$	$0.67 \pm 0.01$	$0.89 \pm 0.01$
		AFE	$0.16 \pm 0.13$	$33.78 \pm 0.86$	$51.66 \pm 0.74$	$0.04 \pm 0.00$	$0.68 \pm 0.01$	$0.89 \pm 0.01$
		AFI	$1.06 \pm 0.10$	$48.22 \pm 0.78$	$73.32 \pm 0.47$	$0.04 \pm 0.00$	$0.68 \pm 0.01$	$0.89 \pm 0.01$
		AFIO	$1.06 \pm 0.10$	$54.44 \pm 0.78$	$74.16 \pm 0.51$	$0.04 \pm 0.00$	$0.68 \pm 0.01$	$0.89 \pm 0.01$
	0.200	Vanilla	NA	NA	NA	$1.23 \pm 0.11$	$0.71 \pm 0.02$	$0.81 \pm 0.01$
		RF	$6.88 \pm 1.75$	$25.10 \pm 1.01$	$40.60 \pm 0.89$	$1.24 \pm 0.11$	$0.71 \pm 0.02$	$0.81 \pm 0.01$
		AFE	$0.58 \pm 0.36$	$24.48 \pm 0.65$	$38.52 \pm 0.73$	$1.22 \pm 0.11$	$0.71 \pm 0.02$	$0.81 \pm 0.01$
		AFI	$-0.04 \pm 0.58$	$38.72 \pm 0.74$	$60.06 \pm 0.66$	$1.23 \pm 0.11$	$0.71 \pm 0.02$	$0.81 \pm 0.01$
		AFIO	$-0.04 \pm 0.58$	$45.20 \pm 0.93$	$60.84 \pm 0.89$	$1.23 \pm 0.11$	$0.71 \pm 0.02$	$0.81 \pm 0.01$
	0.500	Vanilla	NA	NA	NA	$2.98 \pm 0.28$	$0.73 \pm 0.02$	$0.83 \pm 0.01$
		RF	$19.64 \pm 2.58$	$21.36 \pm 1.59$	$36.82 \pm 1.49$	$3.00 \pm 0.28$	$0.73 \pm 0.02$	$0.83 \pm 0.01$
		AFE	$0.22 \pm 0.87$	$17.48 \pm 0.95$	$26.34 \pm 1.06$	$2.98 \pm 0.28$	$0.73 \pm 0.02$	$0.83 \pm 0.01$
		AFI	$0.98 \pm 1.01$	$27.18 \pm 1.20$	$40.80 \pm 1.27$	$2.97 \pm 0.28$	$0.73 \pm 0.02$	$0.83 \pm 0.01$
		AFIO	$0.98 \pm 1.01$	$33.12 \pm 1.39$	$41.44 \pm 1.57$	$2.97 \pm 0.28$	$0.73 \pm 0.02$	$0.83 \pm 0.01$
	0.005	Vanilla	NA	NA	NA	$0.04 \pm 0.00$	$0.73 \pm 0.02$	$0.93 \pm 0.01$
		RF	$1.20 \pm 0.63$	$28.16 \pm 0.76$	$42.60 \pm 0.90$	$0.04 \pm 0.00$	$0.71 \pm 0.02$	$0.93 \pm 0.01$
		AFE	$0.08 \pm 0.09$	$33.70 \pm 0.79$	$51.64 \pm 0.85$	$0.04 \pm 0.00$	$0.73 \pm 0.02$	$0.93 \pm 0.01$
		AFI	$1.50 \pm 0.32$	$48.90 \pm 0.53$	$74.58 \pm 0.34$	$0.04 \pm 0.00$	$0.73 \pm 0.02$	$0.93 \pm 0.01$
		AFIO	$1.50 \pm 0.32$	$54.50 \pm 0.55$	$74.58 \pm 0.47$	$0.04 \pm 0.00$	$0.73 \pm 0.02$	$0.93 \pm 0.01$
	0.200	Vanilla	NA	NA	NA	$1.14 \pm 0.10$	$0.74 \pm 0.02$	$0.88 \pm 0.01$
		RF	$31.12 \pm 2.79$	$13.04 \pm 1.72$	$29.38 \pm 1.55$	$1.17 \pm 0.10$	$0.74 \pm 0.02$	$0.88 \pm 0.01$
		AFE	$-0.62 \pm 0.57$	$25.84 \pm 1.19$	$38.42 \pm 1.43$	$1.14 \pm 0.10$	$0.74 \pm 0.02$	$0.88 \pm 0.01$
		AFI	$1.10 \pm 0.73$	$41.96 \pm 0.89$	$62.72 \pm 0.85$	$1.14 \pm 0.10$	$0.74 \pm 0.02$	$0.88 \pm 0.01$
		AFIO	$1.10 \pm 0.73$	$48.40 \pm 0.77$	$63.50 \pm 0.72$	$1.14 \pm 0.10$	$0.74 \pm 0.02$	$0.88 \pm 0.01$
	0.500	Vanilla	NA	NA	NA	$2.93 \pm 0.26$	$0.74 \pm 0.02$	$0.89 \pm 0.01$
		RF	$40.68 \pm 2.59$	$7.28 \pm 1.89$	$24.72 \pm 1.73$	$2.97 \pm 0.26$	$0.74 \pm 0.02$	$0.89 \pm 0.01$
		AFE	$2.38 \pm 1.27$	$14.76 \pm 1.25$	$23.68 \pm 1.31$	$2.92 \pm 0.26$	$0.74 \pm 0.02$	$0.89 \pm 0.01$
		AFI	$0.34 \pm 1.14$	$27.98 \pm 1.18$	$41.96 \pm 1.32$	$2.93 \pm 0.26$	$0.74 \pm 0.02$	$0.89 \pm 0.01$
		AFIO	$0.34 \pm 1.14$	$34.50 \pm 0.94$	$42.54 \pm 1.01$	$2.93 \pm 0.26$	$0.74 \pm 0.02$	$0.89 \pm 0.01$
0.30	0.005	Vanilla	NA	NA	NA	$0.05 \pm 0.00$	$0.68 \pm 0.02$	$0.95 \pm 0.01$
		RF	$-2.82 \pm 1.50$	$32.10 \pm 1.09$	$46.06 \pm 1.06$	$0.06 \pm 0.01$	$0.62 \pm 0.02$	$0.95 \pm 0.01$
		AFE	$0.10 \pm 0.40$	$33.80 \pm 0.69$	$51.08 \pm 0.70$	$0.05 \pm 0.00$	$0.68 \pm 0.02$	$0.95 \pm 0.01$
		AFI	$2.30 \pm 0.76$	$49.42 \pm 0.69$	$75.14 \pm 0.45$	$0.05 \pm 0.00$	$0.68 \pm 0.02$	$0.95 \pm 0.01$
		AFIO	$2.30 \pm 0.76$	$55.00 \pm 0.58$	$75.16 \pm 0.36$	$0.05 \pm 0.00$	$0.68 \pm 0.02$	$0.95 \pm 0.01$
	0.200	Vanilla	NA	NA	NA	$1.25 \pm 0.09$	$0.73 \pm 0.02$	$0.93 \pm 0.01$
		RF	$37.16 \pm 2.97$	$13.22 \pm 2.02$	$30.52 \pm 1.77$	$1.33 \pm 0.09$	$0.72 \pm 0.02$	$0.93 \pm 0.01$
		AFE	$-1.76 \pm 0.82$	$28.20 \pm 1.12$	$40.34 \pm 1.19$	$1.25 \pm 0.09$	$0.73 \pm 0.02$	$0.93 \pm 0.01$
		AFI	$-1.66 \pm 1.09$	$48.62 \pm 0.96$	$68.68 \pm 0.74$	$1.26 \pm 0.09$	$0.73 \pm 0.02$	$0.93 \pm 0.01$
		AFIO	$-1.66 \pm 1.09$	$55.26 \pm 0.88$	$68.94 \pm 0.77$	$1.26 \pm 0.09$	$0.73 \pm 0.02$	$0.93 \pm 0.01$
	0.500	Vanilla	NA	NA	NA	$3.27 \pm 0.23$	$0.73 \pm 0.01$	$0.92 \pm 0.01$
		RF	$42.10 \pm 2.85$	$8.34 \pm 2.28$	$26.30 \pm 1.97$	$3.36 \pm 0.24$	$0.72 \pm 0.01$	$0.92 \pm 0.01$
		AFE	$1.44 \pm 1.03$	$16.28 \pm 1.44$	$25.36 \pm 1.42$	$3.27 \pm 0.23$	$0.73 \pm 0.01$	$0.92 \pm 0.01$
		AFI	$1.08 \pm 1.00$	$30.80 \pm 1.21$	$45.56 \pm 1.10$	$3.26 \pm 0.23$	$0.73 \pm 0.01$	$0.92 \pm 0.01$
		AFIO	$1.08 \pm 1.00$	$37.36 \pm 1.22$	$45.72 \pm 1.18$	$3.26 \pm 0.23$	$0.73 \pm 0.01$	$0.92 \pm 0.01$

**Table 4: Performance of Vanilla, RF, and different implementations of AF-CAVI in different simulation scenarios.** For RF, AFE, AFI and AFIO, relative change w.r.t. Vanilla CAVI in iterations ( $\Delta$  Iterations) and (negative) relative change in total and local runtime ( $-\Delta$  Runtime (total) and  $-\Delta$  Runtime (local)) are shown in percentage. For all methods, we show the absolute values of FPR, precision and recall. Values are shown in format mean  $\pm$  standard error.

block ID	block start (bp)	block end (bp)	# of SNPs
1	80841	610729	678
2	610730	2098396	2108
3	2098397	3019660	1216
4	3019661	4348967	1685
5	4348968	5811852	1942
6	5811853	6684885	1020
7	6684886	8347513	2073
8	8347514	9238393	746
9	9238394	11284028	1634
10	11284029	13471127	1538
11	13471128	14486347	916
12	14486348	15648610	1316
13	15648611	16374416	703
14	16374417	18409862	2082
15	18409863	19877471	1126
16	19877472	20905757	624
17	20905758	22732896	1148
18	22732897	23467746	385
19	23467747	28557893	1154
20	28557894	29790947	1071
21	29790948	30727954	1013
22	30727955	32746520	1706
23	32746521	34262952	1483
24	34262953	36469295	2122
25	36469296	37527033	529
26	37527034	40170619	1762
27	40170620	40984601	573
28	40984602	42131573	1046
29	42131574	43862455	972
30	43862456	44744108	704
31	44744109	46102697	1553
32	46102698	47150082	1204
33	47150083	49282227	1985
34	49282228	51532567	2429
35	51532568	52985290	1742
36	52985291	54602362	2530
37	54602363	55728080	1585
38	55728081	57521335	2661
39	57521336	59118839	1403

**Table 5: Start (bp), end (bp) and number of SNPs in each block divided by LDetect (after QC) using the 1000 Genomes Phase 1 Reference panel**